

ภาคผนวก ค

Phase Development, Densification and Dielectric Properties of $(0.95-x)\text{Na}_{0.5}\text{K}_{0.5}\text{NbO}_3 - 0.05\text{LiTaO}_3 - x\text{LiSbO}_3$ Lead-free Piezoelectric Ceramics

Pornsuda Bomlai^{1,*}, Sureewan Sukprasert¹, Supasarute Muensit² and Steven J. Milne³

¹Materials Science Program, and ²Department of Physics, Faculty of Science, Prince of Songkla University, Songkla 90112 Thailand

³Institute for Materials Research, University of Leeds, Leeds LS2 9JT, United Kingdom.

Abstracts

Lead-free piezoelectric ceramics in the system $(0.95-x)\text{Na}_{0.5}\text{K}_{0.5}\text{NbO}_3 - 0.05\text{LiTaO}_3 - x\text{LiSbO}_3$, $x = 0-0.1$, were synthesized by a reaction-sintering method. The effects of the content of LiSbO_3 , and the sintering temperature on phase-development, microstructure and dielectric properties of the samples were investigated. Additions of LiSbO_3 produced a change in crystal system from orthorhombic to tetragonal. The additive reduced the temperature at which secondary recrystallisation occurred, and also affected average grain size, and dielectric constant. A sintering temperature of $1050\text{ }^\circ\text{C}$ (for 2h) was the optimum for this system in order to achieve a high density and high dielectric constant. A maximum dielectric constant of 1510 was recorded for the $x = 0.04$ composition.

KEYWORDS: A. ceramics, B. crystal structure, C. X-ray diffraction, D. dielectric properties, D. microstructure.

* Corresponding e-mail: ppornsuda@yahoo.com
Tel. +66 74 288 250; Fax +66 74 218 701.

1. Introduction

Environmental concerns are stimulating research into the development of lead-free alternative piezoelectric ceramics [1-2]. Mixed alkali niobate-tantalates are leading candidates as replacements for lead zirconate titanate, PZT.

Guo *et al.* [3] investigated the alkali niobate solid solution system $[\text{Na}_{0.5}\text{K}_{0.5}\text{NbO}_3]_{1-x} - [\text{LiTaO}_3]_x$ (abbreviated, NKN-LT) and reported a morphotropic phase boundary (MPB), at $0.05 < x < 0.06$, between orthorhombic and tetragonal phase fields. Compositions close to this MPB gave the highest values of d_{33} piezoelectric charge coefficients in the system, reaching a value of ~ 200 pC/N at $x = 0.05$ with a corresponding Curie temperature (T_c) of ~ 420 °C.

Saito *et al.* [4-5] studied a wider range of related solid solutions, corresponding to the general formula $(\text{K}_{0.5}\text{Na}_{0.5})_{1-x}\text{Li}_x\text{Nb}_{1-y}\text{Ta}_y\text{O}_3$. For a composition, $x = 0.03$ and $y = 0.2$, close to the MPB of this system, d_{33} was 230 pC/N, with a T_c of 323 °C. Reactive template grain growth resulted in enhanced piezoelectric properties, giving values of $d_{33} = 373$ pC/N and $T_c = 323$ °C for $\langle 001 \rangle$ grain-oriented ceramics. Slightly improved values of d_{33} coefficients were obtained using Sb ion doping on the pentavalent sites of the perovskite lattice. These values approach those of some PZT ceramics and consequently have aroused keen interest in developing this compositional system further as a viable Pb-free piezoceramic [6-11].

Although the highest piezoelectric coefficients were demonstrated for textured ceramics fabricated using reactive template grain growth, these fabrication procedures are rather complicated and would be costly for commercial production. Hence it is important to optimize properties in conventional, randomly orientated ceramic samples. For example, Marcos *et al.* [12] have used conventional ceramic processing techniques to

fabricate ceramics of $(K_{0.44}Na_{0.52}Li_{0.04})(Nb_{0.86}Ta_{0.10}Sb_{0.04})O_3$, a composition in the system reported by Saito et al. [4], and also a 'non-stoichiometric' composition $(K_{0.38}Na_{0.52}Li_{0.04})(Nb_{0.86}Ta_{0.10}Sb_{0.04})O_{2.97}$. A higher piezoelectric coefficient was obtained for the latter, with $d_{33} \sim 200$ pC/N.

The present paper addresses phase development, ceramic densification, microstructural evolution and dielectric properties in compositions expressed by the general formula $(0.95-x)Na_{0.5}K_{0.5}NbO_3-0.05LiTaO_3-xLiSbO_3$, made by a mixed-oxide processing route, employing reaction-sintering. The end-member composition, $0.95(Na_{0.5}K_{0.5}NbO_3)-0.05LiTaO_3$ lies near the MPB in the base NKN-LT system.

2. Experimental procedure

Samples were prepared by the conventional mixed-oxide process using K_2CO_3 , Ta_2O_5 (Aldrich Chemical Company, Inc., $\geq 99.0\%$ purity), Na_2CO_3 , Nb_2O_5 (Aldrich Chemical Company, Inc., $99.9+\%$ purity), Li_2CO_3 (Fluka, $>99.0\%$ purity) and Sb_2O_5 (Aldrich Chemical Company, Inc., 99.995% purity), as starting powders. The stoichiometric $Na_{0.5}K_{0.5}NbO_3$ powder was firstly prepared for this system. The two carbonate powders are moisture-sensitive; thermogravimetric analysis indicates that dehydration is completed at ~ 200 °C, therefore to avoid compositional errors when weighing out the $Na_{0.5}K_{0.5}NbO_3$ precursor mixture, the starting reagents were dried in an oven for 24 h prior to use. Dried powders were allowed to cool to room temperature under reduced pressure in a dessicator, and all powders were stored in the dessicator until immediately prior to weighing in the correct proportions. The starting materials were transferred to a 100 mm-diameter cylindrical plastic jar, partially filled with 10 mm-diameter alumina grinding balls. Sufficient ethanol was added to cover the powder/media.

Ball-milling was carried out for 24 h, followed by drying at 120 °C, prior to grinding with an alumina mortar and pestle to break up large agglomerates formed during drying. The mixtures were calcined in alumina crucibles, with loosely fitting lids, at 800 °C for 2 h. The NKN powders were then ground, weighed and ball-milled again for 24 h with Ta₂O₅, Li₂CO₃ (dried) and Sb₂O₅ to obtain the compositions (0.95-x)Na_{0.5}K_{0.5}NbO₃-0.05LiTaO₃ - x LiSbO₃ (abbreviated as NKN-LT-LS) for x = 0.0, 0.02, 0.04, 0.06 and 0.10. A reaction-sintering approach was used to produce the NKN-LT-LS ceramics, in that no second powder calcination stage was employed prior to sintering. The mixed powders were dried, ground and pressed at 100 MPa into 1.5 cm diameter discs and sintered in air at temperature ranging from 1025 - 1150°C for 2 h in closed crucibles.

Ceramic samples were examined at room temperature using X-ray powder diffraction (XRD; Philips X' Pert MPD, Ni-filtered CuK_α radiation) to identify the phase(s) formed. Sintered pellet densities were obtained by the Archimedes method. The microstructures of the as-sintered surfaces of the samples were imaged directly, using scanning electron microscopy (SEM; Jeol : JSM-5800LV). The average grain size was calculated by the mean linear intercept method. To investigate dielectric properties, pellets were electroded with silver paste (SPI Supplies) and capacitance and loss tangents (tan δ) of the samples measured at room temperature using a LCR meter (HP 4263B) at 1 kHz, from which the dielectric constant was calculated.

3. Results and discussion

Figure 1 shows XRD patterns of the (0.95-x)Na_{0.5}K_{0.5}NbO₃-0.05LiTaO₃ - x LiSbO₃ samples which had been sintered at 1050 °C for 2 h. It was found that the phase structure of the product depended significantly on the addition of LiSbO₃. Perovskite

phase was formed in high yield in all samples, but secondary phases appeared. An extra phase, giving faint peaks with a similar pattern to $K_6Li_4Nb_{10}O_{30}$ [13], was detected in all compositions, Fig 1. Residual $LiSbO_3$ [14] was detected in the $x = 0.10$ sample, Fig1.

Further phase analysis was conducted with reference to XRD patterns of a single-phase orthorhombic material (NKN), and of a tetragonal pattern of a 0.94NKN-0.06LT composition, as shown in Figure 3 [15-16]. For the orthorhombic perovskite phase the lower angle peak in the $45-46.5^\circ 2\theta$ pair (highlighted for the $x = 0$ and 0.04 compositions in Figure 2) is the most intense, whilst the reverse holds true for the tetragonal phase. These peaks correspond to (022) and (002) peaks for the orthorhombic phase, and (002) and (200) peaks for the tetragonal phase. Figures 1 and 2 thus indicate the main product phase for the $x = 0$ composition, $0.95Na_{0.5}K_{0.5}NbO_3-0.05LiTaO_3$, to be orthorhombic [3], while all samples with added $LiSbO_3$, $x = 0.02 - 0.10$, showed a tetragonal perovskite solid solution [5]. There was a slight increase in d-spacing between $x = 0$ and $x = 0.02$ samples, for example from 1.994 \AA to 2.010 \AA , for the orthorhombic 022 and tetragonal 002 peaks respectively, Table 1 and Fig 2. However no significant variation in d-spacings were detected for compositions, $x = 0.02-0.1$.

Calculation of the respective peak intensity ratio within the $45-46.5^\circ 2\theta$ pair of peaks (calculated from peak heights) for an orthorhombic NKN 'standard' pattern gives a I_{022}/I_{002} value of ~ 1.3 [15], whilst I_{002}/I_{200} is ~ 0.5 for the 'standard' tetragonal phase [16]. In the present ceramics sintered at $1050^\circ C$, the characteristic XRD pattern of the $x = 0$ composition, gives a peak ratio (I_{022}/I_{002}) of ~ 1.4 , whereas the $LiSbO_3$ modified samples have corresponding values (I_{002}/I_{200}) of $\sim 0.6- 0.8$, Table 1. Although structure factor differences between NKN-LT and NKN-LT-LS solid solutions and those of the selected reference materials will influence specific values, the reference materials

nevertheless provide a basis from which to evaluate the phase content of the experimental samples in detail. The comparative values illustrate that the main product phase for $x = 0$ is solely the orthorhombic NKN-LT phase. However although the LiSbO_3 modification induces a stabilization of the tetragonal polymorph, the actual values of peak ratios (0.6-0.8) are somewhat higher, in relative terms, than for the reference tetragonal pattern (0.5). This suggests that after sintering at $1050\text{ }^\circ\text{C}$ for 2 h there may be some coexisting orthorhombic material along with the predominant tetragonal phase. The net result is a slight increase in intensity ratio from the base tetragonal value of 0.5.

Increasing the sintering temperature to $1075\text{ }^\circ\text{C}$ brought the experimental intensity ratios closer to the values expected from single-phase tetragonal systems for $x = 0.02-0.1$. However there was still a very small amount of LiSbO_3 second phase present in $x = 0.1$, and a small amount of the second phase $\text{K}_6\text{Li}_4\text{Nb}_{10}\text{O}_{30}$ – type structure in all compositions.

A major change in phase content occurred at the highest sintering temperature investigated, $1150\text{ }^\circ\text{C}$, Figs 2 and 4. The tetragonal pattern was replaced by a pattern similar to that of cubic perovskite. This probably is indicative of partial melting occurring at $1150\text{ }^\circ\text{C}$.

The variation in densities of the $(0.95-x)\text{Na}_{0.5}\text{K}_{0.5}\text{NbO}_3-0.05\text{LiTaO}_3-x\text{LiSbO}_3$ ceramics for different sintering temperatures, is shown in Fig 5. It was found that density was very sensitive to slight changes in sintering temperature. The highest density samples were produced at a sintering temperature of $1050\text{ }^\circ\text{C}$. This is around $50\text{ }^\circ\text{C}$ lower than required for ceramics of related compositions prepared by full calcination prior to sintering [16], indicating the effectiveness of the reaction sintering approach. Density values were $4.32 \pm 0.01\text{ g/cm}^3$ for a sample with $x = 0.0$, increasing gradually with

increasing amounts of LiSbO_3 giving a value of $4.44 \pm 0.01 \text{ g/cm}^3$ for a sample with $x = 0.10$. This trend may reflect the higher mass of Sb. Indeed recalling that some LiSbO_3 was detected in the $x = 0.1$ sample at $1050 \text{ }^\circ\text{C}$, the higher density of LiSbO_3 ($\sim 5.45 \text{ g/cm}^3$) will increase the measured density of this sample, Fig 5. At $1075 \text{ }^\circ\text{C}$, the ceramic densities were $\sim 2\%$ lower than at $1050 \text{ }^\circ\text{C}$; this trend generally continued with further $25 \text{ }^\circ\text{C}$ increments in sintering temperature, Fig 5. However for the highest LiSbO_3 samples, $x = 0.1$, and to a lesser extent, $x = 0.06$, the density fell more rapidly with rising sintering temperature. This is attributed to structural changes, and possible melting (Figure 5). For all sample compositions, an increase in volatilisation losses, particularly of Li and K [16] and possibly Sb at temperatures $> 1050 \text{ }^\circ\text{C}$ may contribute to the observed gradual decrease in measured densities with increasing temperature

The microstructures of samples sintered at temperatures ranging from $1050 - 1100 \text{ }^\circ\text{C}$ showed that grain size and shape depended strongly on sintering temperature and on LiSbO_3 content, Figs 6-8. For a sintering temperature of $1050 \text{ }^\circ\text{C}$, the $x = 0$ and $x = 0.02$ compositions each showed grain sizes $< 1 \text{ } \mu\text{m}$, however at $x = 0.04$ a change to much larger maximum grain sizes, and a distribution typical of secondary recrystallisation was evident, Fig 6. This mechanism produced cuboid grains with maximum grain sizes $\sim 5 \text{ } \mu\text{m}$ in a fine grained matrix, Fig 6c,d.

At $1075 \text{ }^\circ\text{C}$ all compositions, $x = 0.02-0.1$, showed secondary recrystallisation. Maximum grain sizes were $\sim 8 \text{ } \mu\text{m}$ for $x = 0$. A slight decrease in grain size was observed with increasing LiSbO_3 content. Sintering at $1100 \text{ }^\circ\text{C}$ produced a maximum grain size of $\sim 12 \text{ } \mu\text{m}$ in the $x = 0$ sample. Again the trend of decreasing grain size with increasing LiSbO_3 substitution was observed.

Variations in *average* grain size, as calculated by the linear intercept method, are shown in Fig 9. There was a marked discontinuity in the 1050 °C plot between $x = 0.02$ and 0.04 due to the change in grain growth mechanism. A gradual decrease in average size with increasing x is evident for higher sintering temperatures, where all compositions exhibit secondary recrystallisation.

In other perovskites such as BaTiO_3 , secondary recrystallisation is often thought to be associated with liquid phase formation. A similar mechanism leading to bimodal grain size distributions may occur in the NKN-LT-LS system. Changes in microstructure with increasing temperature, and increasing LiSbO_3 content, may relate to changes in the amount and composition of any liquid phase.

Dielectric properties of dense samples, sintered at temperatures ranging from 1050 – 1100 °C, are shown in Fig 10. The dielectric constant of the $x = 0$, NKN sample was ~ 600-700 for the full range of sintering temperatures studied, 1050-1100 °C. This value is higher than that reported in previous studies for $0.95\text{Na}_{0.5}\text{K}_{0.5}\text{NbO}_3$ - 0.05LiTaO_3 [17] or for NKN ceramics sintered at 1110 °C [3].

The incorporation of LiSbO_3 brought about substantial increases in the dielectric constant. Values were a maximum of 1510 for the $x = 0.04$ starting composition, sintered at 1050 °C, Fig 10. Values for $x = 0.02$ and 0.06 were also relatively high, 1300-1350, for this sintering temperature, but the $x = 0.1$ sample had a much lower value, similar to that of $x = 0$. The latter effect may be due to the presence of unreacted LiSbO_3 . A dielectric constant of 1510 for $x = 0.04$ is very close to that reported for textured ceramics of $(\text{K}_{0.44}\text{Na}_{0.52}\text{Li}_{0.04})(\text{Nb}_{0.86}\text{Ta}_{0.10}\text{Sb}_{0.04})\text{O}_3$ for which the value reached 1570 [4], and is much higher than values reported for alkali niobate tantalate (NKN-LT) compositions produced by conventional calcination and sintering [3, 7].

Sintering at higher temperatures, 1075 °C or 1100 °C produced lower dielectric constants than for the 1050 °C samples, which may relate to their lower densities. For all compositions, the value was between ~ 800-1000. Dissipation factors for the LiSbO₃ - modified samples were higher than expected, varying between ~ 0.1-0.7. The highest value occurred for the x = 0.04 sample sintered at 1050 °C. One possible reason for the high dissipation factors may be a high electrical conductivity, which could be related to alkali oxide (or antimony oxide) losses during sintering. However oxide volatilisation would increase with increasing sintering temperature, yet the dissipation factors were lower, ~ 0.5, for the x = 0.04 ceramics sintered at 1075 °C and 1100 °C.

4. Conclusions

Small increments to sintering temperature, and changes to the amount of LiSbO₃ strongly affect phase content, densification, microstructure and dielectric properties of (0.95-x)Na_{0.5}K_{0.5}NbO₃-0.05LiTaO₃-xLiSbO₃ ceramics. The additive promotes the formation of a tetragonal crystal structure, as opposed to the orthorhombic structure of the 0.95Na_{0.5}K_{0.5}NbO₃-0.05LiTaO₃ end-member. The reaction-sintering approach employed produces maximum densities of 4.3-4.4 g/cm³ for a sintering temperature of only 1050 °C. This is a lower temperature than is usually reported for ceramics of related compositions fabricated using full powder calcination before sintering. A composition 0.91(Na_{0.5}K_{0.5})NbO₃ - 0.05LiTaO₃ - 0.04LiSbO₃ sintered at 1050 °C shows the highest dielectric constant in this system, with a room -temperature value of ~1510. Raising the sintering temperature from 1050 °C to 1075 °C, produced ceramics with ~ 2 % lower density and dielectric constants were reduced in value to ~ 1000.

Acknowledgments

This work was supported by Thailand Research Fund (TRF) and Commission on Higher Education.

References

1. European Council, Official Journal of the European Union. L37 (2003) 19-23.
2. IEEE: IEEE Standard on Piezoelectricity, ANSI/IEEE Standard No. 176 IEEE, New York (1987).
3. Guo, K. Kakimoto, and H. Ohsato, *Mater. Lett.* 59 (2005) 241-244.
4. Y. Saito, H. Takao, I. Tani, T. Nonoyama, K. Takatori, T. Homma, T. Nagaya, and M. Nakamura, *Nature*. 432 (2004) 84-87.
5. Y. Saito and H. Takao, *Ferroelectrics*. 338 (2006) 17-32.
6. R. Zuo, J. Rödel, R. Chen, and L. Li, *J. Am. Ceram. Soc.* 89 (2006) 2010-2015.
7. E. Hollenstein, M. Davis, D. Damjanovic, and N. Setter, *Appl. Phys. Lett.* 87(182905) (2005) 1-3.
8. J-F. Li, K. Wang, B-P. Zhang and L-M. Zhang, *J. Am. Ceram. Soc.* 89 (2006) 706-709.
9. R. Wang, R-J. Xie, K. Hanada, K. Matsusaki, H. Bando, and M. Itoh, *Phys. Stat. Sol.* 202 (2005)R57-R59.
10. B-P. Zhang, J-F. Li, K. Wang, and H. Zhang, *J. Am. Ceram. Soc.* 89 (2006) 1605-1609.
11. G-Z. Zang, J-F. Wang, H-C. Chen, W-B. Su, C-M. Wang, P. Qi, B-Q. Ming, J. Du, L-M. Zheng, S. Zhang, and T. R. ShROUT, *Appl. Phys. Lett.* 88 (2006) 212908-212911.
12. F. R-Marcos, P. Ochoa, J. F. Fernandez, *J. Eur. Ceram. Soc.* (2007) in press.

13. Powder Diffraction File No. 48-0997, International Centre for Diffraction Data, Newton Squire, PA, 2001.
14. Powder Diffraction File No. 84-2003, International Centre for Diffraction Data, Newton Squire, PA, 2001.
15. P. Bomlai, P. Wichianrat, S. Muensit and S. J. Milne, *J. Am. Ceram. Soc.* 90 (2007) 1650-1655.
16. T. A. Skidmore, S. J. Milne, *J. Mater. Res.* (2007) in press.
17. M.-S. Kim, D.-S. Lee, E.-C. Park, S.-J. Jeong and J.-S. Song, *J. Eur. Ceram. Soc.* (2007) in press.

List of Table

Table I XRD data showing d - spacings and intensity ratios as a function of x (the LiSbO_3 content) and sintering temperatures.

List of Figures

Fig.1 XRD patterns of samples $(0.95-x)[\text{Na}_{0.5}\text{K}_{0.5}\text{NbO}_3-0.05\text{LiTaO}_3] - x \text{LiSbO}_3$ sintered at $1050\text{ }^\circ\text{C}$ for 2 h (* = $\text{K}_6\text{Li}_4\text{Nb}_{10}\text{O}_{30}$ [13]; \blacktriangledown = LiSbO_3 [14]).

Fig. 2 XRD patterns in the 2θ range of $44-47^\circ$ for $0.95\text{Na}_{0.5}\text{K}_{0.5}\text{NbO}_3-0.05\text{LiTaO}_3$ sample ($x = 0$) sintered at $1050\text{ }^\circ\text{C}$ (a); and $0.91\text{Na}_{0.5}\text{K}_{0.5}\text{NbO}_3-0.05\text{LiTaO}_3 - 0.04\text{LiSbO}_3$ samples ($x = 0.04$) sintered at different temperatures for 2 h: (b) $1050\text{ }^\circ\text{C}$ (c) $1075\text{ }^\circ\text{C}$ and (d) $1150\text{ }^\circ\text{C}$.

Fig. 3 comparison of XRD patterns for orthorhombic $(\text{Na}_{0.5}\text{K}_{0.5})\text{NbO}_3$ powder calcined at $900\text{ }^\circ\text{C}$ [15] and tetragonal $0.94(\text{Na}_{0.5}\text{K}_{0.5})\text{NbO}_3-0.06\text{LiTaO}_3$ powder calcined at $1100\text{ }^\circ\text{C}$ [16].

Fig. 4 XRD patterns in the 2θ range of $20-60^\circ$ for $0.91(\text{Na}_{0.5}\text{K}_{0.5})\text{NbO}_3-0.05\text{LiTaO}_3-0.04\text{LiSbO}_3$ ($x = 0.04$) sintered at 1075 and $1150\text{ }^\circ\text{C}$.

Fig. 5 The density values of samples $(0.95-x)[\text{Na}_{0.5}\text{K}_{0.5}\text{NbO}_3-0.05\text{LiTaO}_3] - x \text{LiSbO}_3$ when sintered at different temperatures.

Fig. 6 SEM micrographs $(1-x)[\text{Na}_{0.5}\text{K}_{0.5}\text{NbO}_3 - 0.05\text{LiTaO}_3] - x \text{LiSbO}_3$ samples where x is : a) 0; b) 0.02; c) 0.04 and d) 0.10 sintered at $1050\text{ }^\circ\text{C}$ for 2 h.

Fig. 7 SEM micrographs $(1-x)[\text{Na}_{0.5}\text{K}_{0.5}\text{NbO}_3-0.05\text{LiTaO}_3] - x \text{LiSbO}_3$ samples where x is : a) 0; b) 0.02; c) 0.04 and d) 0.10 sintered at $1075\text{ }^\circ\text{C}$ for 2 h.

Fig. 8 SEM micrographs $(1-x)[\text{Na}_{0.5}\text{K}_{0.5}\text{NbO}_3-0.05\text{LiTaO}_3] - x \text{LiSbO}_3$ samples where x is : a) 0; b) 0.02; c) 0.04 and d) 0.10 sintered at 1100 °C for 2 h.

Fig.9 Average grain size of $(0.95-x)[\text{Na}_{0.5}\text{K}_{0.5}\text{NbO}_3-0.05\text{LiTaO}_3] - x \text{LiSbO}_3$ samples when sintered at various temperatures for 2 h

Fig. 10 Dielectric constant of $(0.95-x) [\text{Na}_{0.5}\text{K}_{0.5}\text{NbO}_3-0.05\text{LiTaO}_3 - x \text{LiSbO}_3$ samples

Table I XRD data showing *d*- spacings and intensity ratios as a function of x (the LiSbO₃ content) and sintering temperatures.

LiSbO ₃ content, x (mole)	Sintering temperature (°C)	<i>d</i> -spacings (Å)		I ₀₂₂ /I ₀₀₂	I ₀₀₂ /I ₂₀₀
		022/002	002/200		
0.00	1050	1.994	1.966	1.38	-
	1075	2.003	1.971	1.69	-
0.02	1050	2.010	1.972	-	0.62
	1075	2.014	1.975	-	0.56
0.04	1050	2.006	1.972	-	0.78
	1075	2.011	1.974	-	0.58
0.06	1050	2.002	1.969	-	0.71
	1075	2.005	1.973	-	0.56
0.10	1050	2.004	1.972	-	0.72
	1075	2.004	1.973	-	0.48

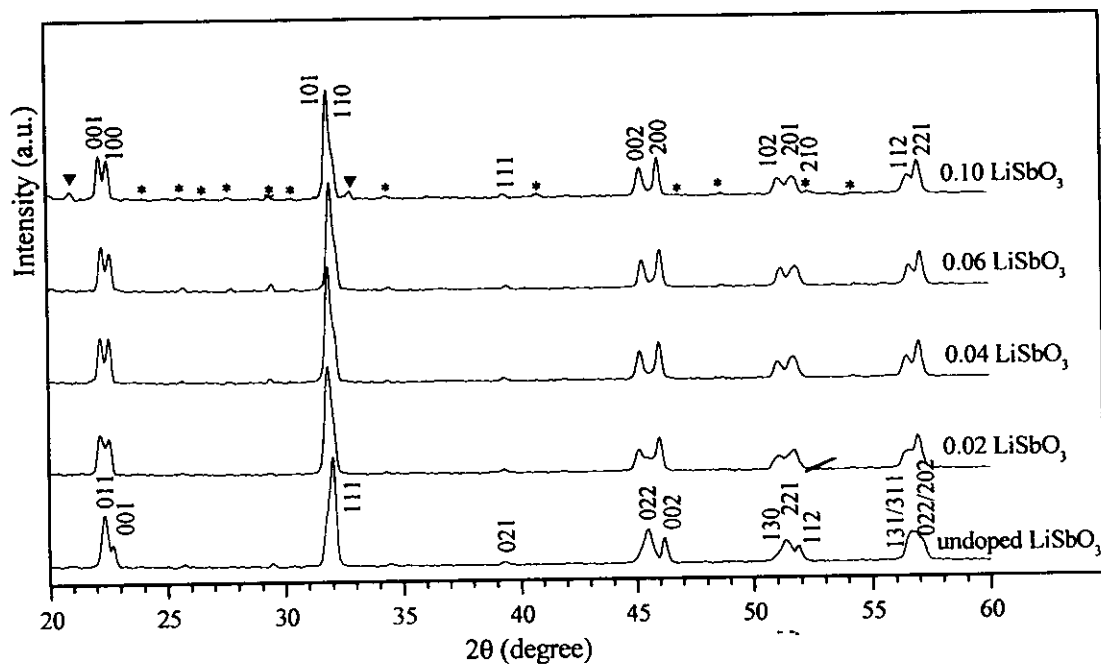


Fig.1

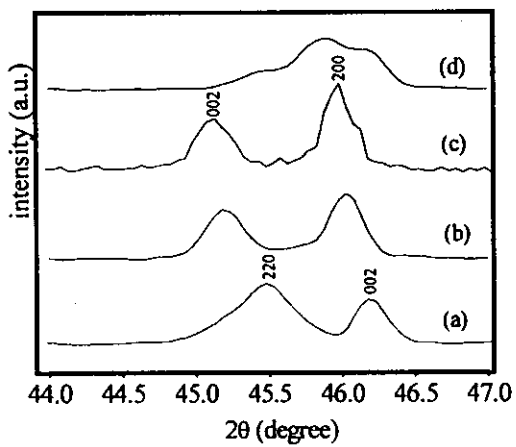


Fig. 2

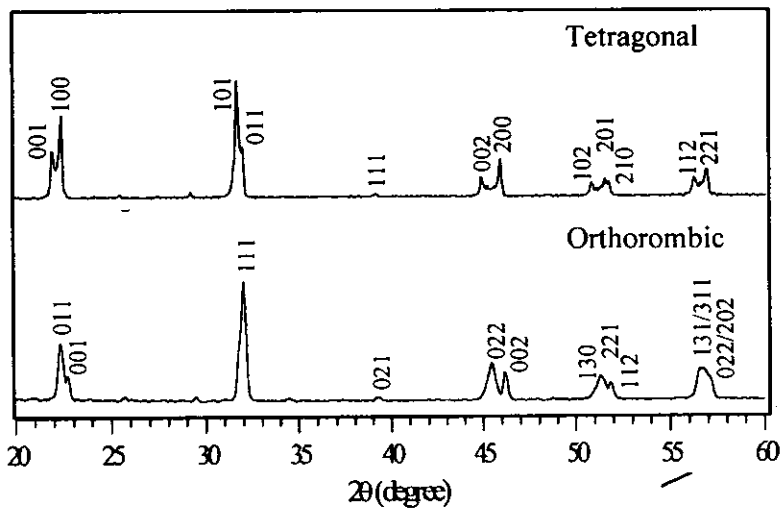


Fig. 3

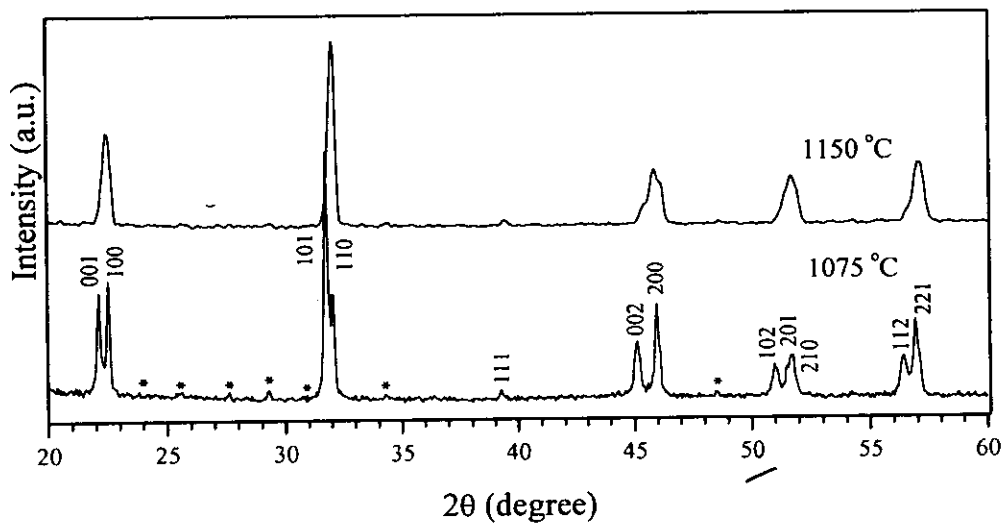


Fig. 4

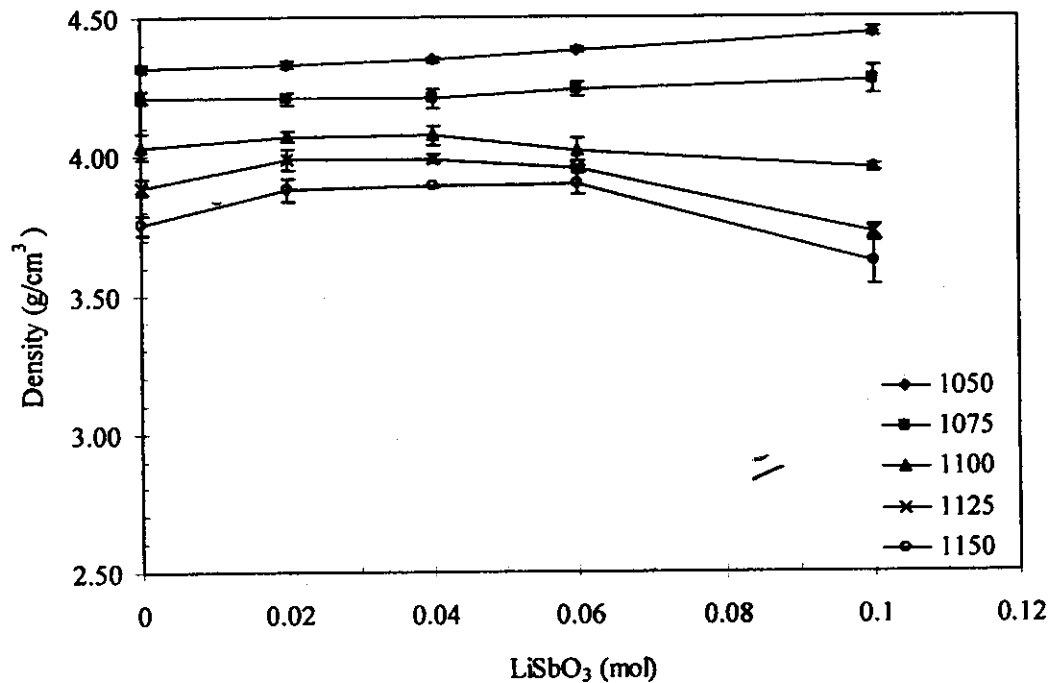


Fig. 5

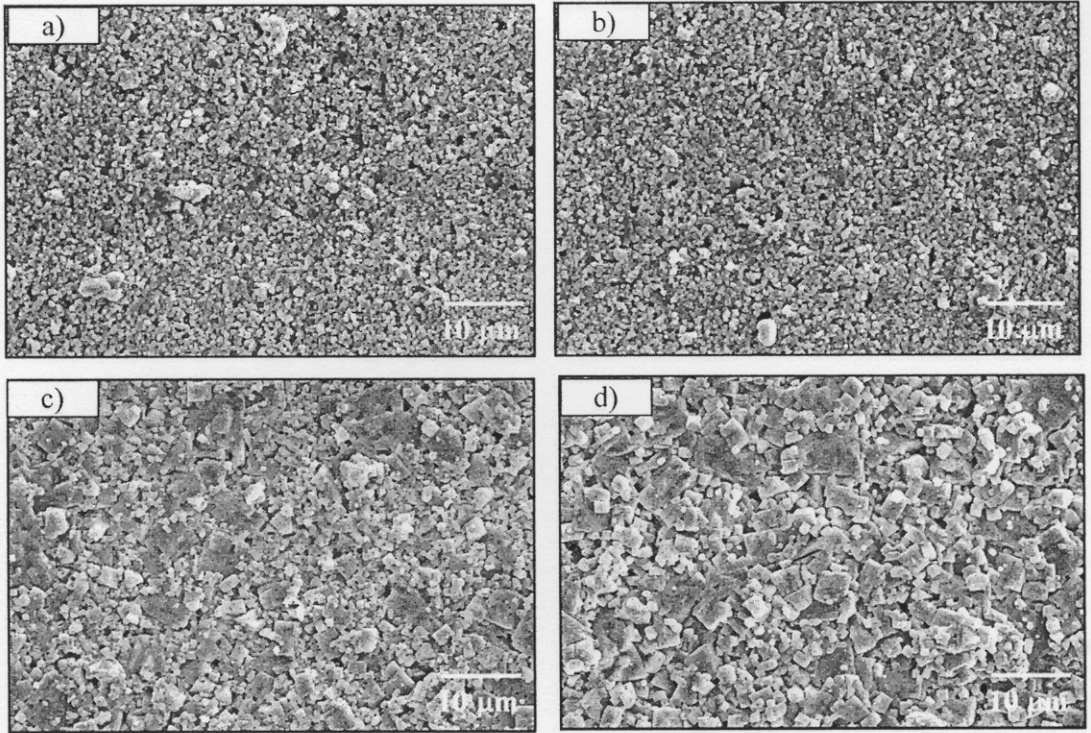


Fig. 6

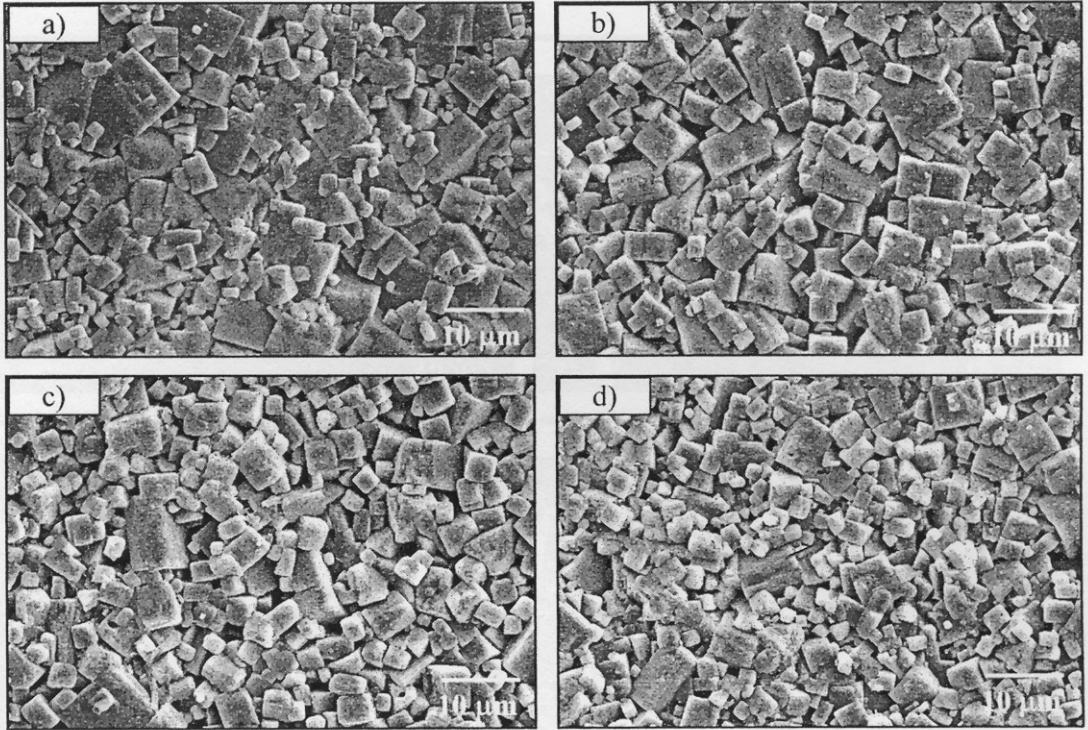


Fig. 7

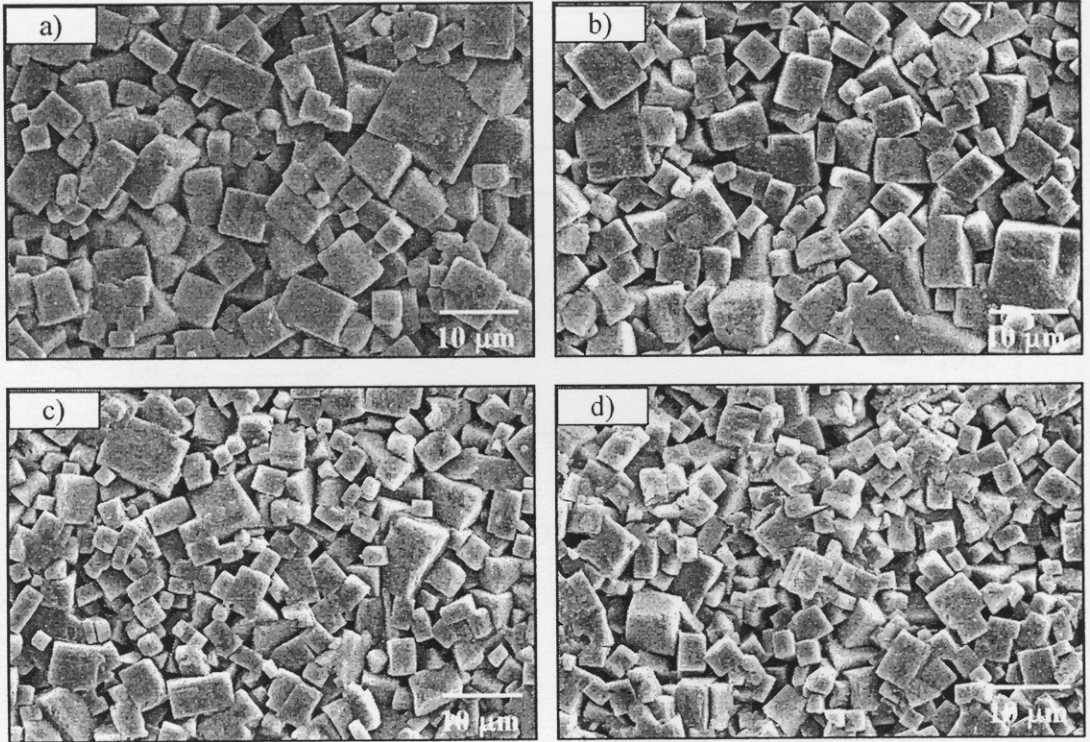


Fig. 8

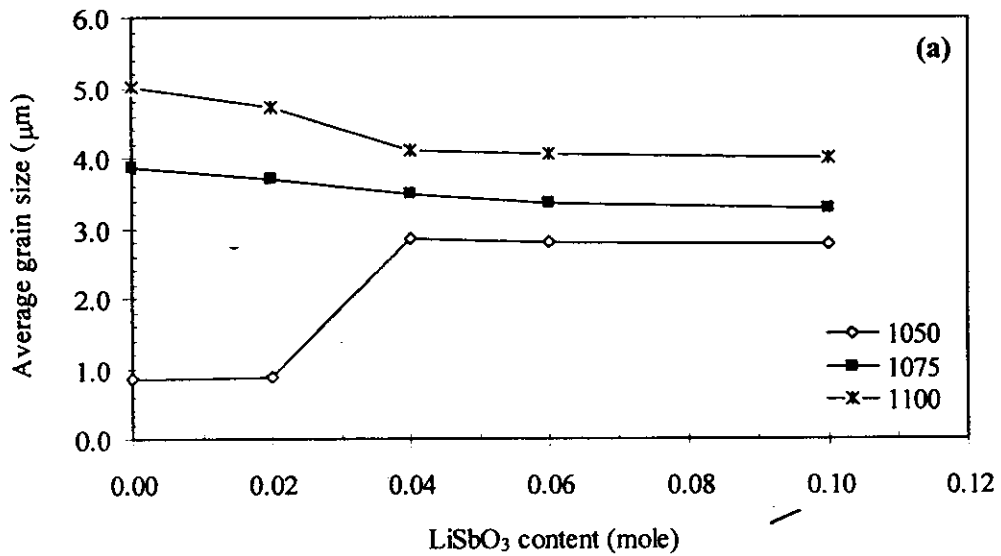


Fig.9

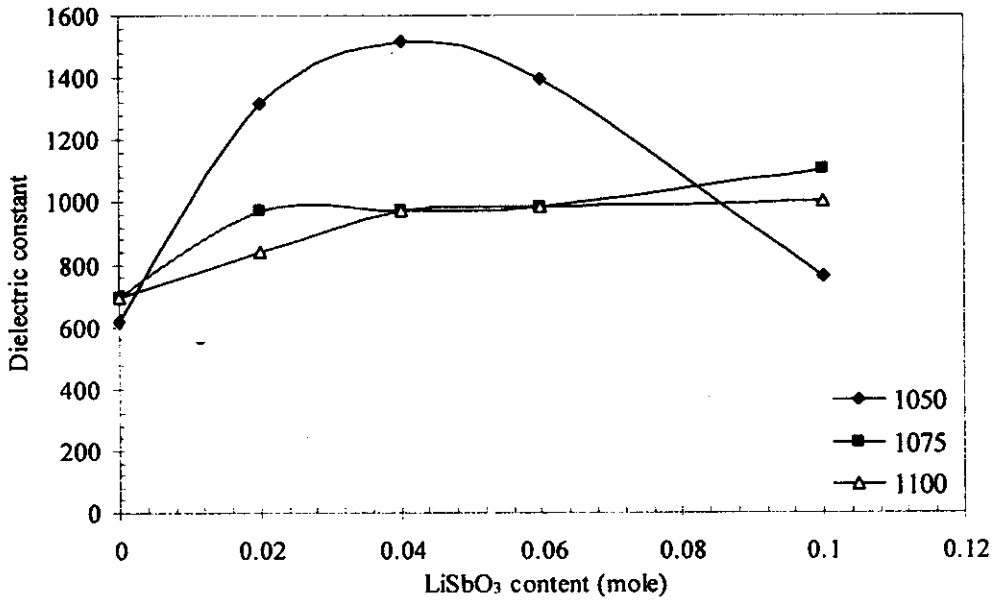


Fig. 10